Impedance spectroscopy analysis of zirconia:8 mol% yttria solid electrolytes with graphite pore former

R. Muccillo[a)]
CMDMC—Center of Science and Technology of Materials, Energy and Nuclear Research Institute, S. Paulo, SP 05422-970, Brazil

(Received 13 August 2008; accepted 15 January 2009)

Porous ZrO_2:8 mol% Y_2O_3 sintered ceramics were prepared by adding graphite powder as pore former before sintering. The thermal elimination of graphite was evaluated by thermogravimetric analysis. Impedance spectroscopy analysis was carried out in the 5 Hz to 13 MHz frequency range in specimens sintered with and without pore former. The deconvolution of the impedance diagrams, $[Z''(\omega) \times Z'(\omega)]$ and $[Z''(\omega) \times \log f]$, and the numerical residuals resulting from the subtraction of normalized impedance spectroscopy diagrams measured in specimens with and without pore formers were evaluated. A comparison of the impedance diagrams of samples sintered with and without pore former shows evidence of a modification of the electrical response caused by pores. The results show the unequivocal ability of the impedance spectroscopy technique to gauge microstructural modification caused by the presence of pores in ionic conducting solids.

I. INTRODUCTION

ZrO_2:8 mol% Y_2O_3 polycrystalline ceramics are one of the most important electroceramic materials mainly because of their electrical properties above room temperature. They are largely used in commercial devices such as lambda oxygen sensors (for measuring the partial pressure of oxygen in gas exhaust and to optimize the air–fuel ratio in combustion engine vehicles for less fuel consumption and for pollution depletion) and in solid oxide fuel cells (as dense oxide ion conductor solid electrolyte, as porous cermet anode with Ni, and as porous composite cathode with lanthanum strontium manganite).

Sintered polycrystalline ceramic materials consist basically of grains and interfaces, the latter being mainly composed of grain boundaries, segregated impurities, and pores. In oxide ions conducting solid electrolytes, the interfaces contribute to the reduction of the total electrical conductivity of a system by blocking charge carriers, oxide ion vacancies, at these intergranular regions. The grain boundaries in oxide ion conductors, which consist of one grain-boundary core and two adjacent space charge layers, are blockers to O^{2-} charge carriers because of oxygen vacancy depletion in the space charge layer, and the blocking intensity decreases as the temperature increases.[1–6] Pores are supposed to block the ionic transport across the grain boundaries by decreasing the conduction path width and constricting current lines, similar to the effect of impurities at grain boundaries.[7]

The impedance spectroscopy technique consists of applying to the electrode/specimen/electrode cell a low-amplitude alternating voltage $V = V_0\, e^{j\omega t}$, where ω is the pulsation and V_0 the voltage signal amplitude. The current output is $I = I_0\, e^{j(\omega t+\phi)}$, where ϕ is the phase angle of the current versus voltage and I_0 is the current signal amplitude. The impedance is $Z(\omega) = V/I = Z_0\, e^{-j\phi} = Z'(\omega) + j\, Z''(\omega)$, where Z' and Z'' are the real and the imaginary components and $Z_0 = V_0/I_0 = |\, Z(\omega)\, |$. Usually $-Z''$ is plotted as a function of Z', the plot being composed of one or more semicircles, either superposed or not, which may be assigned to different contributions to the electrical resistivity due to the bulk (grains) and to interfaces (mainly grain boundaries) of the polycrystalline ceramics.[6–8] This technique has been used extensively to separate bulk and interfacial contributions (e.g., grain boundary) and electrode effects from the overall response of solid electrolytes to an applied ac electrical signal.[7] Depending on the temperature and on the frequency range used in the impedance spectroscopy experiment, the impedance spectroscopy diagram $[-Z''(\omega) \times Z'(\omega)]$ in the complex plane usually presents two visually separated semicircles,[6–8] each represented by an equivalent circuit composed of a resistor in parallel with a constant phase element (CPE) when the center of these semicircles lies below the Z' axis.[13] The impedance of a CPE is given by $Z_{CPE} = Q^{-1}(j\omega)^{-\alpha}$, $0 \leq \alpha \leq 1$.[7] The high-frequency semicircle is usually attributed to the electrical response of the bulk of the polycrystalline specimen, whereas the low-frequency semicircle is assumed to represent the electrical properties of the highly resistive grain boundaries. Then the impedance

[a)]Address all correspondence to this author.
e-mail: muccillo@usp.br
DOI: 10.1557/JMR.2009.0209

spectroscopy technique allows, at least to a first approximation, the separation of impedance contributions from grain interior (bulk) and grain boundaries.[6–8,14,15]

Polycrystalline ceramics may be prepared either porosity-free or with a controlled degree of porosity depending on the application. Porous ceramics are widely used in a series of devices such as filtration membranes and electrodes in solid oxide fuel cells. Similar to porosity-free ceramics, those with a controlled volume of pores must also be dense, with high skeletal density, for supporting mechanical loads under service. Porous ceramics are prepared by several processing techniques including chemical synthesis, e.g., sol-gel, sacrificial organic pore formers,[16–18] polymeric foam templates, etc., each with their advantages. The porosity evaluation of ceramics is usually done with experiments in a mercury intrusion porosimeter or by observation of polished and etched surfaces by electron microscopy (scanning and/or transmission). Porous ceramics behave electrically in a different manner compared with porosity-free ceramics. The pores may be considered volume defects that somehow impede the transport of charge, acting as blockers.[18] The current lines resulting from the external applied electric field may follow detours around the pores, giving rise to a modification in the low-frequency region of the impedance diagrams of solid electrolytes. In other words, the mean free path of the charge carriers across the specimen submitted to an applied electric field is larger in a porous region of the specimen than in a dense region. This behavior, namely the modification in the impedance diagram in the low-frequency region, has already been reported for cracks in zirconia solid electrolytes,[19] for insulating monoclinic phase in partially stabilized zirconia–magnesia solid electrolytes,[20] for insulating regions in (zirconia–yttria) + yttria composites,[21] for the deviation of the idealized brick layer model,[9–12] and for nonhomogeneous lithium conductive ceramics.[22] In this work, we take advantage of the possibility of separating the contributions to the electrical conductivity of solid electrolytes due to bulk and interfaces to the study of pores in zirconia–yttria solid electrolytes, taking into account that intergranular pores may modify the intergranular electrical response. The main results indicate that a detailed numerical analysis of impedance spectroscopy data allows for evaluating the contribution of pores to the alternating current (AC) electrical response of solid electrolytes.

II. EXPERIMENTAL

Commercially available nanometric powders of zirconia stabilized with 8 mol% yttria (Tosoh TZ-8Y, Tosoh Corporation, Tokyo, Japan) was used. The powders were dried, weighed, and pressed to 10 mm diameter to 2 mm thickness pellets at 90 MPa. Pores were introduced to the specimens by adding 1 wt% graphite powder with >99.9% carbon and 9.9 m^2/g specific surface area from Nacional de Grafite Ltda., Brazil, before mixing and pressing for sintering in air at 1500 °C for 2 h, with an additional presintering step performed at 600 °C for 1 h for elimination of the graphite. The heating rate was 2 °C/min to facilitate the reaction of the graphite with air to release carbon dioxide. Some sintered pellets were broken up in small fragments to allow for mercury intrusion under increasing pressure during the evaluation of the distribution of pore sizes in a mercury porosimeter Autopore from Micromeritics (Norcross, GA).

Fracture surfaces of TZ-8Y sintered with and without graphite were observed in a Quanta Inspect F FEI (Hillsboro, OR) scanning electron microscope.

Thermogravimetric experiments were performed in the ZrO_2:8 mol% Y_2O_3 + 1.0 wt% C in a Setaram (Caluire, France) thermal analyzer to follow the graphite elimination.

Impedance spectroscopy measurements were carried out at 400 °C in sintered cylindrical pellets with a 1492 LF Hewlett Packard (Tokyo, Japan) impedance analyzer in the 5 Hz to 13 MHz frequency range with an input signal of 200 mV for improved signal-to-noise ratio. Data with measurements applying 50 and 100 mV gave the same impedance diagrams showing that all measurements were in the linear ohmic region. The samples had their parallel surfaces coated with silver paste and cured at 200 °C/5 min for removal of the organic binder. The samples, three similar compositions at a time, were inserted in an Inconel 600 sample chamber with alumina insulators and platinum leads, and a type K thermocouple with its tip close to the samples. The sample chamber was positioned inside a Lindberg-Blue M (Watertown, WI) furnace with temperature control within ±0.5 °C at the samples location. The $[-Z''(\omega) \times Z'(\omega)]$ data were collected and analyzed with special software[23] using a series 362 HP Controller running on a HP Basics operational system. This software allows for the deconvolution of multisemicircle impedance diagrams either by regression analysis of the fitted data or by the sequence (i) plotting one semicircle, (ii) subtracting from the whole diagram, and (iii) plotting the remaining diagram. For plotting, the data had to be converted to text data with a HP LiF software. Before coating with silver paste, the flat surface of the specimens was analyzed by x-ray diffraction in a D8 Advance diffractometer (Bruker-AXS, Karlsruhe, Germany), θ–2θ Bragg–Brentano configuration, with Cu Kα radiation with 40 kV to 40 mA, 20° to 80° 2θ range, 0.05° step size, 5 s counting time per step.

III. RESULTS AND DISCUSSION

Figure 1 shows the variation of the weight of the mixture of ZrO_2:8 mol% Y_2O_3 with 1 wt% graphite

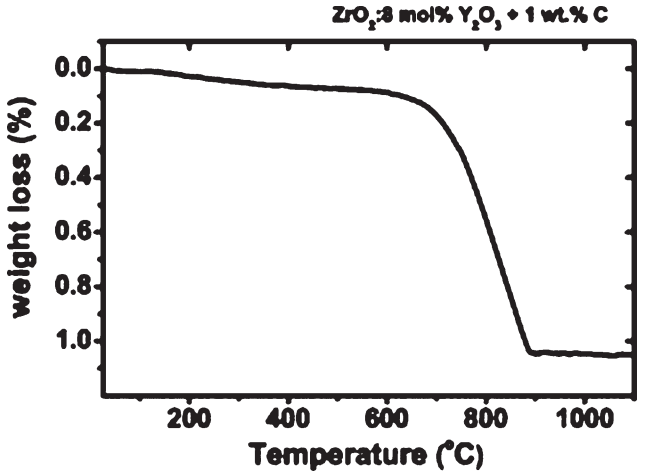

FIG. 1. Thermogravimetric curve of ZrO_2:8 mol% Y_2O_3 + 1 wt% C; heating rate 10 °C/min; atmosphere: air.

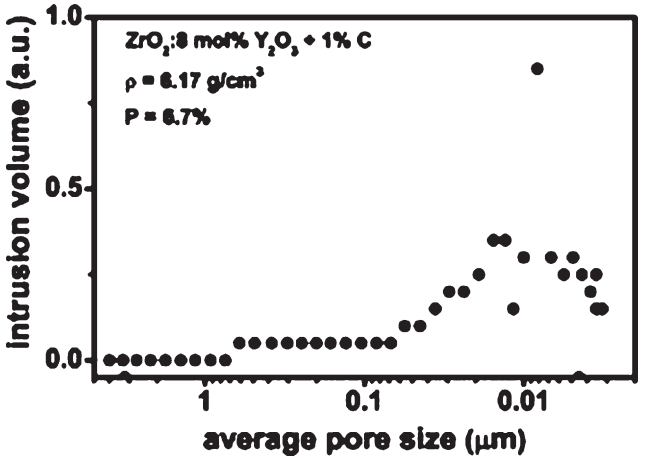

FIG. 2. Pore-size distribution in ZrO_2:8 mol% Y_2O_3 sintered with 1 wt% graphite.

upon heating at 10 °C/min in air from room temperature to 1100 °C. The weight loss starts at approximately 600 °C and ends at approximately 890 °C, corresponding to the graphite elimination.

The pressed pellets of the ZrO_2:8 mol% Y_2O_3 + 1 wt% C mixture sintered at 1500 °C/2 h were analyzed by mercury porosimetry. The results are shown in Fig. 2. These results are an average of measurements in several fracture pieces of the pellets. Pore size values are distributed in the 0.06–0.003 μm range, centered at approximately 0.01 μm. The value of the density is 6.17 $g \cdot cm^{-3}$, which corresponds to 93.3% of the theoretical density. The sintered specimen with 5.7% pore volume has high skeletal density.

The flat surface of ZrO_2:8 mol% Y_2O_3 with 1% graphite sintered pellets were also analyzed by x-ray diffraction. The results show that the porous sintered pellet is single phase with fluorite cubic phase, according to the JCPDS file No. 81-1551.

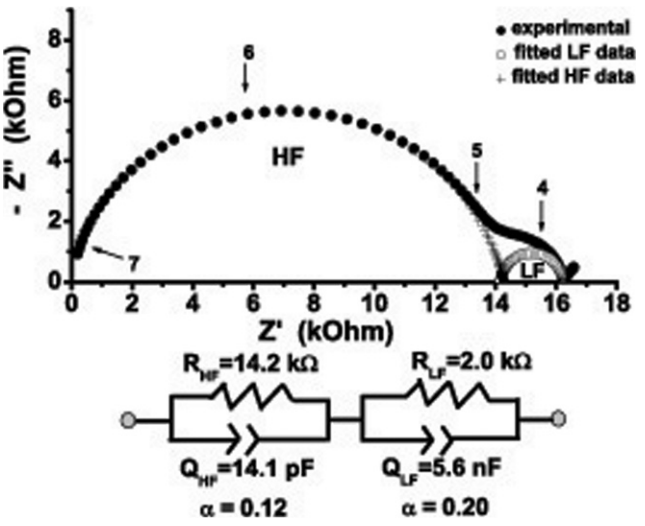

FIG. 3. Impedance diagram of ZrO_2:8 mol% Y_2O_3 sintered ceramic, measured at 400 °C. Numbers stand for the logarithm of frequency of the applied signal. Bottom: electrical equivalent circuit.

The impedance spectroscopy measurements of the ZrO_2:8 mol% Y_2O_3 pellets sintered without and with 1% graphite were carried out in the 300 to 500 °C range, which is part of the oxide ion conductivity domain. Figure 3 shows the $[-Z''(\omega) \times Z'(\omega)]$ impedance spectroscopy diagram measured at 400 °C in the 5 Hz to 13 MHz frequency range of a ZrO_2:8 mol% Y_2O_3 pellet sintered at 1500 °C/2 h. The deconvolution of the impedance diagram shows that it is composed by two well-defined semicircles, extensively reported in the literature: a high-frequency (HF) semicircle from the intragranular or bulk component of the impedance and a low-frequency (LF) semicircle from the intergranular or grain boundary component of the impedance.[6–8] The impedance spectroscopy diagram may be modeled by a resistor in parallel with a constant phase element ($R_{HF} \parallel Q_{HF}$), representing the bulk response, in series with another resistor in parallel with a capacitor ($R_{LF} \parallel Q_{LF}$), representing the grain boundaries response. Figure 3 also depicts the electrical equivalent circuit.

Figure 4 shows the impedance diagram of ZrO_2:8 mol% Y_2O_3 + 1% graphite pellets sintered at 1500 °C/2 h. Pores have been formed with the distribution shown in Fig. 2. The impedance diagram is similar to that of the ZrO_2:8 mol% Y_2O_3 sintered without pore former, but presents a distortion in the 10^4 to 5×10^5 Hz intermediate frequency range. Moreover, the deconvolution program shows that besides the high-frequency and low-frequency semicircles, another semicircle may be resolved at an intermediate-frequency (IF) range. The only difference between both specimens is the presence of pores in the specimen sintered with addition of graphite before pressing and sintering. The IF semicircle is

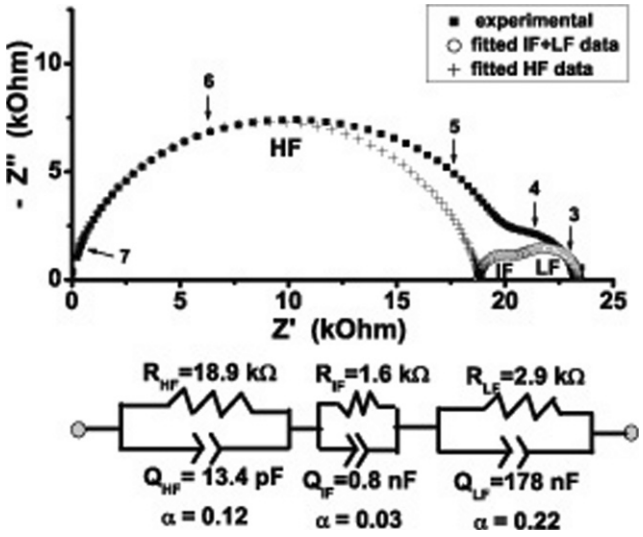

FIG. 4. Impedance diagram of ZrO_2:8 mol% Y_2O_3 + 1 wt% C sintered ceramic at 400 °C. Numbers stand for the logarithm of frequency of the applied signal. Bottom: electrical equivalent circuit.

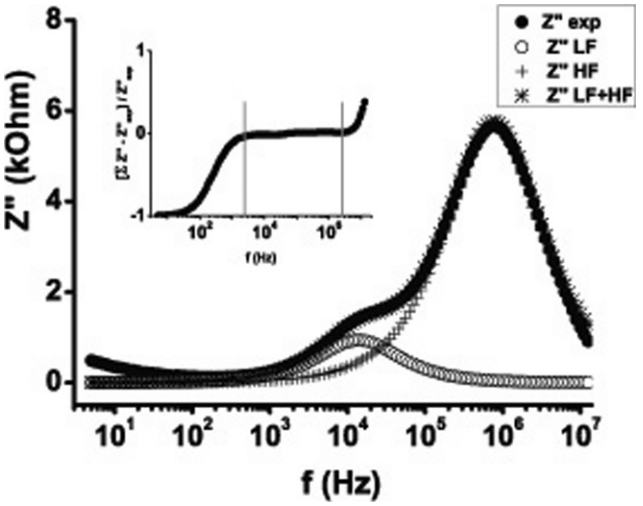

FIG. 5. Bode reactance diagram of ZrO_2:8 mol% Y_2O_3 sintered ceramic at 400 °C with the deconvolution into the two bottom curves. Inset: percentage variation of the difference between the sum of the deconvoluted curves and the experimental result.

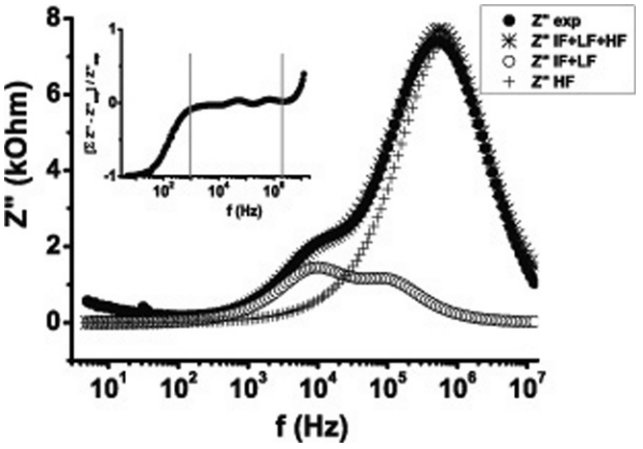

FIG. 6. Bode reactance diagram of ZrO_2:8 mol% Y_2O_3 + 1 wt% C sintered ceramic at 400 °C with the deconvolution into the two bottom curves. Inset: percentage variation of the difference between the sum of the deconvoluted curves and the experimental result.

then ascribed to pores, which may be acting as blockers to oxygen vacancies. The modeling using electrical equivalent circuit, in this case, is represented by an additional resistor in parallel with a constant phase element ($R_{IF} \parallel Q_{IF}$), now representing the pores. Figure 4 shows also this electrical equivalent circuit.

Some data could be extracted from Figs. 3 and 4. After the deconvolution of the impedance diagram, the capacitances of all components are estimated: C(HF) = 13.4 pF/cm, C(IF) = 0.8 nF/cm, and C(LF) = 178 nF/cm. The LF capacitance is approximately 10^4 times the HF capacitance as expected for grain-boundary capacitance (LF) relative to the bulk capacitance (HF). In other words, the average grain size is approximately 10^4 times larger than the average intergranular distance. The IF capacitance, assigned to the pore contribution, is approximately 60 times the HF capacitance. In other words, the average grain size is approximately 60 times larger than the average pore size. Or the average pore size is two orders of magnitude larger than the average intergranular distance.

Additional evidence that the deconvolution of the impedance diagram enables us to show an electrical response because of the presence of pores is discussed, plotting the Bode reactance diagram of both specimens, sintered with and without pore former. Figure 5 shows the Bode reactance diagram, $[Z''(\omega) \times \log f]$ of the ZrO_2:8 mol% Y_2O_3 solid electrolyte. Data, collected at 400 °C, shows unequivocally the presence of two relaxation processes, corresponding to the LF and HF responses, which are shown in the figure after the deconvolution of the overall diagram. The inset shows the adequacy of the fitting: the mean deviation between the experimental data and the sum of the fitted data is less than 1%, except at the extremities of the data (extreme high and extreme low frequencies) where the experimental data are prone to larger errors, but do not exceed 1%. The high-frequency deviation is caused by the contribution of an inductance caused by the 1 m coaxial cable, known to occur at high-frequency/low-resistance values in the impedance analyzers. The low-frequency deviation is caused by the electrode contribution to the impedance diagram.

The same procedure was followed for the analysis of the Bode reactance diagram of the ZrO_2:8 mol% Y_2O_3 solid electrolyte sintered with pore former. The results are shown in Fig. 6.

Figure 6 shows clearly that the Bode reactance diagram of the ZrO_2:8 mol% Y_2O_3 sintered with pore former may

also be resolved into three components, related to the HF, IF, and LF semicircles depicted in Fig. 4. The best fit is found for using the three components, and the inset shows that the mean deviation between experimental and calculated data is below 1%. The deviations in the low-frequency and high-frequency ends of the diagram result from the same causes as stated previously.

IV. CONCLUSIONS

The impedance spectroscopy technique was successfully used to study the porous zirconia–yttria solid electrolytes. It has been shown that pores give rise to an additional electrical response in the impedance diagrams, corresponding to a relaxation process probably associated to pores acting as blockers to charge carriers (O^{2-} ions). This response could be easily evaluated by determining the mean square deviation of the difference, on a frequency basis, between the impedance diagrams measured in specimens sintered with and without pore former. The impedance spectroscopy technique has been shown to be an important tool in the study of porous ceramic materials conditioned to their electrical behavior. In the sequence, the impedance spectroscopy technique will be used to study porous ZrO_2:8 mol% Y_2O_3-NiO composites before and after reduction of NiO under hydrogen, a material used as an anode in solid oxide fuel cells.

ACKNOWLEDGMENTS

The author acknowledges FAPESP (Proc. 05/53241-9) for financial support and Dr. F.C. Fonseca and Dr. D. Gouvêa for thermal analysis and porosimetry measurements, respectively.

REFERENCES

1. X. Guo and R. Waser: Electrical properties of the grain boundaries of oxygen ion conductors: Acceptor-doped zirconia and ceria. *Prog. Mater. Sci.* **51,** 151 (2006).
2. M.J. Verkerk, B.J. Middelhuis, and A.J. Burggraaf: Effect of grain-boundaries on the conductivity of high-purity ZrO_2–Y_2O_3 ceramics. *Solid State Ionics* **6,** 159 (1982).
3. X. Guo: Physical origin of the intrinsic grain-boundary resistivity of stabilized-zirconia—Role of the space-charge layers. *Solid State Ionics* **81,** 235 (1995).
4. X. Guo: Solute segregations at the space-charge layers of stabilized zirconia: An opportunity for ameliorating conductivity. *J. Eur. Ceram. Soc.* **16,** 575 (1996).
5. D. Bingham, P.W. Tasker, and A.N. Cormack: Simulated grain-boundary structures and ionic-conductivity in tetragonal zirconia. *Philos. Mag. A* **60,** 1 (1989).
6. J.E. Bauerle: Study of solid electrolyte polarization by a complex admittance method. *J. Phys. Chem. Solids* **30,** 2657 (1969).
7. E. Barsoukov and J.R. Macdonald: *Impedance Spectroscopy, Theory, Experiment, and Applications*, 2nd ed. (John Wiley & Sons, Hoboken, NJ, 2005).
8. M. Kleitz, H. Bernard, E. Fernandez, and E. Schouler: Impedance spectroscopy and electrical resistance measurements on stabilized zirconia, in *Advances in Ceramics, Vol. 3, Science and Technology of Zirconia*, edited by A.H. Heuer and L.W. Hobbs (The American Ceramic Society, Columbus, OH, 1981), p. 310.
9. J. Fleig and J. Maier: A finite element study on the grain boundary impedance of different microstructures. *J. Electrochem. Soc.* **145,** 2081 (1998).
10. J. Fleig and J. Maier: Finite-element calculations on the impedance of electroceramics with highly resistive grain boundaries: I, Laterally inhomogeneous grain boundaries. *J. Am. Ceram. Soc.* **82,** 3485 (1999).
11. J. Fleig: The influence of non-ideal microstructures on the analysis of grain boundary impedances. *Solid State Ionics* **131,** 117 (2000).
12. J. Fleig: The grain boundary impedance of random microstructures: Numerical simulations and implications for the analysis of experimental data. *Solid State Ionics* **150,** 181 (2002).
13. G.J. Brug, A.L.G. Van der Eeden, M. Sluyters-Rehbach, and J.H. Sluyters: The analysis of electrode impedances complicated by the presence of a constant phase element. *J. Electroanal. Chem.* **176,** 275 (1984).
14. S.P.S. Badwal: Grain-boundary resistivity in zirconia-based materials: Effect of sintering temperatures and impurities. *Solid State Ionics* **76,** 67 (1995).
15. R.W. Rice: *Porosity of Ceramics* (Marcel Dekker, New York, 1998).
16. R.W. Rice: *Ceramic Fabrication Technology* (Marcel Dekker, New York, 2003).
17. J.S. Woyansky, C.E. Scott, and W.P. Minnear: Processing of porous ceramics. *Am. Ceram. Soc. Bull.* **71,** 1674 (1992).
18. L. Dessemond, R. Muccillo, M. Hénault, and M. Kleitz: Electric conduction-blocking effects of voids and second phases in stabilized zirconia. *Appl. Phys. A* **57,** 57 (1993).
19. M. Kleitz, C. Pescher, and L. Dessemond: Impedance spectroscopy of microstructure defects and crack characterization, in *Science and Technology of Zirconia V*, edited by S.P.S. Badwal, M.J. Bannister, and R.H.J. Hannink (Technomic Publishing, Lancaster, PA, 1993), p. 593.
20. E.N.S. Muccillo and M. Kleitz: Impedance spectroscopy of Mg-partially stabilized zirconia and cubic phase decomposition. *J. Eur. Ceram. Soc.* **16,** 453 (1996).
21. F.C. Fonseca and R. Muccillo: Impedance spectroscopy analysis of percolation in (yttria-stabilized zirconia)-yttria ceramic composites. *Solid State Ionics* **166,** 157 (2004).
22. M. Vijayakumar and O. Bohnke: The current detour effect observed on materials with random microstructure: Experimental evidence from $Li_{3x}La_{2/3-x}TiO_3$ studied by impedance spectroscopy. *J. Eur. Ceram. Soc.* **26,** 3221 (2006).
23. M. Kleitz and J.H. Kennedy: Resolution of multicomponent impedance diagrams, in *Fast Ion Transport in Solids*, edited by P. Vashishta, J.N. Mundy, and G.K. Shenoy (Elsevier North Holland, The Netherlands, 1979), p. 185.